CrystEngComm

PAPER

View Article Online
View Journal | View Issue

Cite this: *CrystEngComm*, 2023, **25**, 2119

Modulated self-assembly of hcp topology MOFs of Zr/Hf and the extended 4,4′-(ethyne-1,2-diyl) dibenzoate linker†

Sophia S. Boyadjieva,[a] Francesca C. N. Firth,[b] Mohammad R. Alizadeh Kiapi,[c] David Fairen-Jimenez,[c] Sanliang Ling,[d] Matthew J. Cliffe *[e] and Ross S. Forgan *[a]

Received 10th November 2022,
Accepted 26th February 2023

DOI: 10.1039/d2ce01529c

rsc.li/crystengcomm

Careful control of synthetic conditions can enhance the structural diversity of metal–organic frameworks (MOFs) within individual metal-linker combinations. Herein, we show that **hcp** topology MOFs of both Zr(IV) and Hf(IV), linked by the extended (ethyne-1,2-diyl)dibenzoate linker, can be prepared by modulated self-assembly. The controlled addition of acetic acid and water to solvothermal syntheses is essential to generate these phase pure **hcp** topology materials, which are characterised experimentally and computationally. The central alkyne unit of the linker can be quantitatively brominated, but this results in partial degradation of the **hcp** phase, in contrast to the more stable **fcu** topology analogues. Nevertheless, the MOFs represent new members of the **hcp** topology isoreticular series showing high crystallinity and porosity, and demonstrate that new materials can be discovered in existing MOF phase spaces through judicious adjustment of key synthetic parameters.

Introduction

Metal–organic frameworks (MOFs) comprise metal ion or metal cluster nodes (also referred to as secondary building units, or SBUs) connected by multitopic organic ligands into multidimensional network structures.[1] To date, it is estimated that over 100 000 MOF structures have been deposited in the Cambridge Structural Database,[2] with this huge number attributed to the chemical diversity in the choice of both metal SBU and organic ligand.[3] In addition, it is possible to isolate multiple phases from the same metal–ligand combination—topological diversity—by careful control of reaction parameters.[4] A pertinent example is that of trivalent metals linked by linear ditopic dicarboxylates, which can yield structurally rigid (MIL-101) and flexible (MIL-88 and MIL-53) phases.[5] Furthermore, we have also previously shown that, in the specific case of Fe(III) MOFs with 1,4-benzenedicarboxylate (BDC^{2-}), coordination modulation—the addition of reagents to MOF syntheses that can tune the coordination and pH equilibria during self-assembly[6]—is a viable strategy for kinetically selecting a specific material from a complex phase landscape.[7]

The multiple series of MOFs comprising Zr(IV) or Hf(IV) SBUs connected by linear ditopic dicarboxylate ligands present a particularly striking case study into the isolation of different MOF phases *via* synthetic control.[8] Predominant among MOFs prepared from Zr(IV) or Hf(IV) and BDC^{2-} or its derivatives is the UiO-66 series, in which $[M_6(\mu_3\text{-}O)_4(\mu_3\text{-}OH)_4(RCO_2)_{12}]$ metal clusters (M = Zr, Hf, Fig. 1a) are connected by twelve linear dicarboxylate linkers in a face-centred cubic (**fcu**) topology MOF (Fig. 1b). UiO-66(Zr) specifically exhibits the ideal formula $[Zr_6O_4(OH)_4(BDC)_6]$,[9] and a wide range of isoreticular derivatives of these materials, including interpenetrated UiO-66 topology phases, have been reported with both longer and functionalised linkers.[9–15]

Varying the reaction composition can also affect the resultant MOF structure. For example, changing the metal source from $ZrCl_4$ to $Zr(^iOPr)_4$ has led to the discovery of a polymorph of UiO-66 with a different connectivity and **hex** topology.[16] Addition of monotopic carboxylic acids as coordination modulators has induced formation of "defect" phases where the modulators themselves are incorporated as charge-compensating defects. Such defect phases can form in

[a] *WestCHEM School of Chemistry, University of Glasgow, Joseph Black Building, University Avenue, Glasgow G12 8QQ, UK. E-mail: ross.forgan@glasgow.ac.uk*
[b] *Yusuf Hamied Department of Chemistry, University of Cambridge, Cambridge CB2 1EW, UK*
[c] *The Adsorption & Advanced Materials Laboratory (A2ML), Department of Chemical Engineering & Biotechnology, University of Cambridge, Philippa Fawcett Drive, Cambridge CB3 0AS, UK*
[d] *Advanced Materials Research Group, Faculty of Engineering, University of Nottingham, University Park, Nottingham NG7 2RD, UK*
[e] *School of Chemistry, University of Nottingham, University Park, Nottingham, NG7 2RD, UK. E-mail: matthew.cliffe@nottingham.ac.uk*

† Electronic supplementary information (ESI) available. See DOI: https://doi.org/10.1039/d2ce01529c

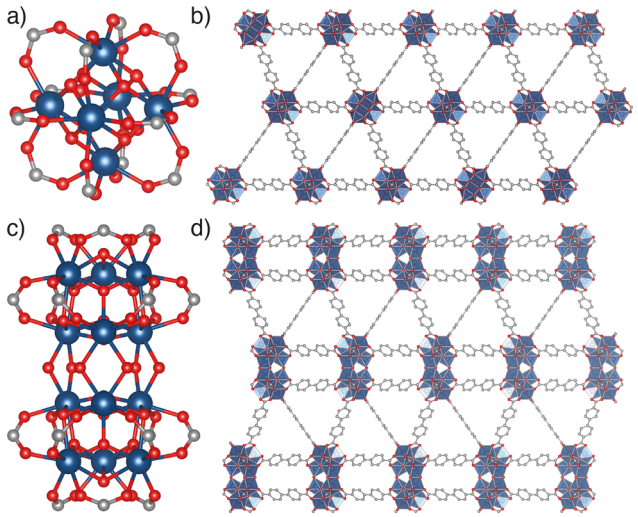

Fig. 1 Comparison of the **fcu** and **hcp** topology MOFs adopted by tetravalent metals and linear dicarboxylate linkers, specifically focussing on those of Hf(IV) and biphenyl-4,4′-dicarboxylate (BPDC). a) The $[Hf_6(\mu_3\text{-}O)_4(\mu_3\text{-}OH)_4(RCO_2)_{12}]$ SBU. b) A section of the packing structure of **fcu** topology $[Hf_6O_4(OH)_4(BPDC)_6]$, also known as UiO-67(Hf). c) The $[Hf_{12}(\mu_3\text{-}O)_8(\mu_3\text{-}OH)_8(\mu_2\text{-}OH)_6(RCO_2)_{18}]$ SBU. d) A section of the packing structure of **hcp** topology $[Hf_{12}O_8(OH)_{14}(BPDC)_9]$. Hf: blue spheres (or, demonstrating Hf coordination environments in SBUs, polyhedra); C: grey; O: red. H atoms omitted for clarity.

MOFs with the linker 2,6-naphthalenedicarboxylate, where the connectivity of the hexanuclear SBU is reduced by the presence of charge-capping, monotopic acetate units.[17] Modulated synthesis can even lower the connectivity of the structure in an ordered manner, as seen in the formation of **reo** UiO-66, which can be described as a missing cluster defect phase, where modulator incorporation (for example formic acid) leads to eight-connected SBUs that form well-defined nanodomains of the missing-cluster defect phase **reo** within the bulk of **fcu** UiO-66.[18,19] Increasing reaction temperatures leads to the MIL-140 series of MOFs phase, which have an infinite one-dimensional chain SBU.[20] MIL-140A, linked by BDC^{2-}, is representative of the isoreticular series, having overall formula [ZrO(BDC)]. It is suggested that the presence of a condensed 1-D chain SBU and its isolation at higher reaction temperatures means that MIL-140A is the thermodynamic phase and UiO-66 is a kinetic product,[20] although addition of water to syntheses promotes UiO-66 formation.[21]

Further careful synthetic control[22] enables the synthesis of MOFs with higher nuclearity Zr(IV) or Hf(IV) SBUs linked by ditopic dicarboxylates.[23–27] For example, MOFs containing the condensed $[M_{12}(\mu_3\text{-}O)_8(\mu_3\text{-}OH)_8(\mu_2\text{-}OH)_6(RCO_2)_{18}]$ SBU (Fig. 1c) and adopting the **hcp** topology (Fig. 1d) have been reported with a range of linkers, including BDC^{2-} and functionalised derivatives,[28–33] 1,4-naphthalenedicarboxylate,[29] and longer linkers such as biphenyl-4,4′-dicarboxylate,[23,30,34] 1,1′:4′,1″-terphenyl-4,4″-dicarboxylate,[35,36] 4,4′-di(4-benzoato)-2,2′-bipyridine,[37] and 5,15-di(*p*-benzoato)porphyrin.[38] An example using poly(ethylene terephthalate) as the source of the BDC^{2-} linker *via* direct synthesis has also been described.[39] Individual systems have also been shown to undergo delamination by sonication, forming a hexagonal layered (**hxl**) phase and eventually hexagonal nanosheets (**hns**),[23] which can also in specific cases be directly synthesised themselves.[30]

The **hcp** topology MOFs have been increasingly studied due to potential applications in luminescence,[29] water remediation,[31] heterogeneous catalysis,[32,33,35] photocatalysis,[37] nanomedicine,[38] and molecular separations.[39] Herein, we describe the synthesis and characterisation of Zr(IV) and Hf(IV) analogues of the **hcp** phase MOF linked by 4,4′-(ethyne-1,2-diyl)dibenzoate (EDB^{2-}), which we have termed GUF-12 (GUF = Glasgow University Framework), by careful control of acetic acid and water content in solvothermal syntheses in DMF. We show the syntheses are scaleable, and that the MOFs have high porosity. Their metastability is demonstrated through efforts to postsynthetically modify them by bromination of their internal alkyne units, which, in the case of the Hf analogue, results in partial delamination or degradation.

Results and discussion

During attempts to prepare nanoparticulate versions of **fcu** topology Zr(IV) MOFs[13,40] as part of our investigations into drug delivery,[41] it was found that addition of high quantities of acetic acid and water to DMF-based solvothermal syntheses containing $ZrCl_4$ and EDB-H_2 resulted in formation of a new phase. This new MOF, termed GUF-12(Zr), was suspected to be the **hcp** analogue due to its characteristic hexagonal plate morphology and the nature of its powder X-ray diffractogram.

The optimal conditions to isolate the **hcp** phases of both the Zr(IV) and Hf(IV) congeners of GUF-12 were identified *via* modulated solvothermal self-assembly. Specifically, 0.34 mmol each of MCl_4 (M = Zr or Hf) and EDB-H_2 (prepared according to a modified literature protocol[13,42]) were combined in 15 ml DMF, with addition of 75 μL deionised water (0.5% v/v) and 2.12 mL acetic acid (37.1 mmol, or 110 equiv. compared to the metal ion). The mixture was heated to 150 °C overnight in a PTFE-lined stainless steel autoclave, and the product isolated by centrifugation once cooled. Both the deliberate addition of water, and the use of a specific quantity of acetic acid as modulator, were key to ensure isolation of the **hcp** phases rather than the **fcu** analogue or other materials (see ESI,† Section S2). These observations tally with our previous mechanistic study that describes how the addition of large amounts of carboxylate modulator to syntheses is required to form the classical $[M_6O_4(OH)_4]$ clusters found in the **fcu** phases, while concomitant addition of water induces cluster merging to form the $[M_{12}O_8(OH)_{14}]$ units that comprise the **hcp** phases.[22] Increasing water content in syntheses containing Hf(IV) and $BPDC^{2-}$ has previously led to the isolation of the **hns** phase over the **hcp** analogue,[30] but with the EDB^{2-} linker only **hcp** phase

materials were formed when water content in syntheses was increased while retaining 110 equiv. of added acetic acid. In contrast, reducing the amount of acetic acid modulator in syntheses occasionally resulted in the failure to produce a MOF.

Even with careful optimisation of the synthesis conditions, single crystals large enough for characterisation by single crystal X-ray diffraction were unable to be grown for either GUF-12 analogue. SEM analysis showed formation of micron-scale hexagonal plates <100 nm in depth that are aggregated into a "desert rose" morphology, which is characteristic of MOF materials with this **hcp** topology (Fig. 2a and b).[30] The structure of these materials was therefore determined by a combination of powder X-ray diffraction analysis and the use of model structures derived from density functional theory (DFT) calculations. Structural models of the **hcp** phase were constructed from the parent **fcu** phase, and then geometry-optimised by DFT calculations using the CP2K code (see ESI,† Section S3). These optimised structures confirmed the kinetic stability of the **hcp** topology models for the Zr(IV) and Hf(IV) analogues.

Qualitative comparison of the powder X-ray diffractograms calculated from these DFT-derived **hcp** structures with those found experimentally (as well as those calculated from the crystal structures of the **fcu** phases) clearly indicate that GUF-12(Zr) and GUF-12(Hf) adopt the **hcp** topology (Fig. 2c).

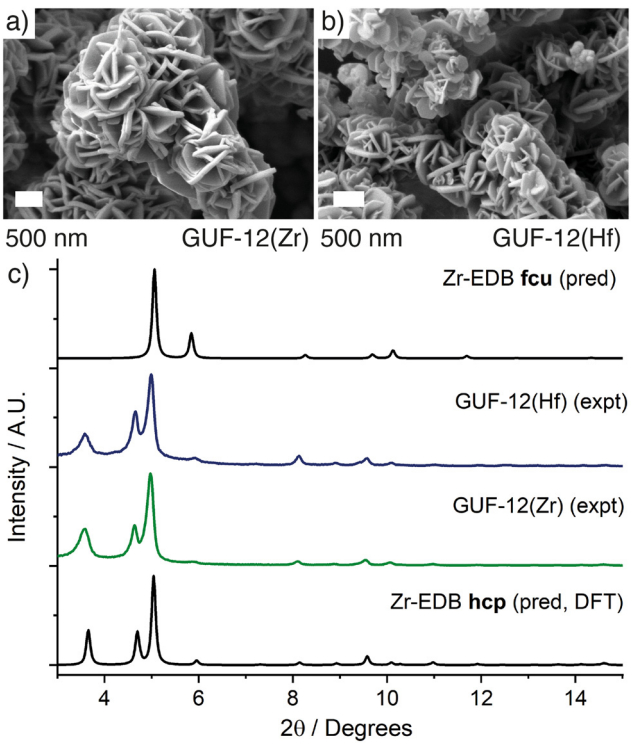

Fig. 2 Scanning electron micrographs of the desert rose morphology of a) GUF-12(Zr) and b) GUF-12(Hf). c) Stacked powder X-ray diffractograms of GUF-12(Zr) and GUF-12(Hf) compared to patterns predicted for the **hcp** phase, derived from DFT model structures, and for the **fcu** phase, derived from the single crystal structures.[13]

Quantitative Pawley fitting of the diffractograms (see ESI,† Section S4) in space group $P6_3/mmc$, using the Topas Academic 6.0 software package,[43] confirmed that these materials were phase pure, and allowed accurate determination of the lattice parameters of these materials: GUF-12(Zr) a = 21.6121(31) Å, c = 48.014(12) Å; GUF-12(Hf) a = 21.5349(32) Å, c = 47.869(13) Å (Fig. 3). The DFT-optimised lattice parameters were within 0.6% of the experimental parameters. We also note that GUF-12(Hf) has a slightly smaller unit cell than GUF-12(Zr), due to slightly shorter Hf–O bonds.

Bulk composition was also assessed by thermogravimetric analysis (TGA) of the GUF-12 samples after activation at 120 °C for 20 h under turbomolecular pump vacuum to remove residual solvents (Fig. 4a). The metal oxide residue remaining after heating in air to 800 °C is indicative of metal content in the pristine MOF. For both GUF-12(Zr) and GUF-12(Hf), the residues were slightly higher than would be predicted for a pristine **hcp** phase; 42.1% wt for GUF-12(Zr) (theoretical: 40.8% wt) and 56.8% wt for GUF-12(Hf) (theoretical: 54.1% wt). These values suggest that the **fcu** phase is not significantly present in either case as the **hcp** phase has a higher overall metal weight percentage than the analogous **fcu** phase (theoretical residues of 34.9% wt and 47.8% wt would be expected for the pristine Zr(IV) and Hf(IV) **fcu** phases, respectively). Furthermore, these TGA results suggest that the **hcp** phases may exhibit some missing linker defects (replacement of EDB^{2-} linkers by smaller charge-compensating acetates reduces the relative organic content in the MOF, increasing the metal weight percentage and

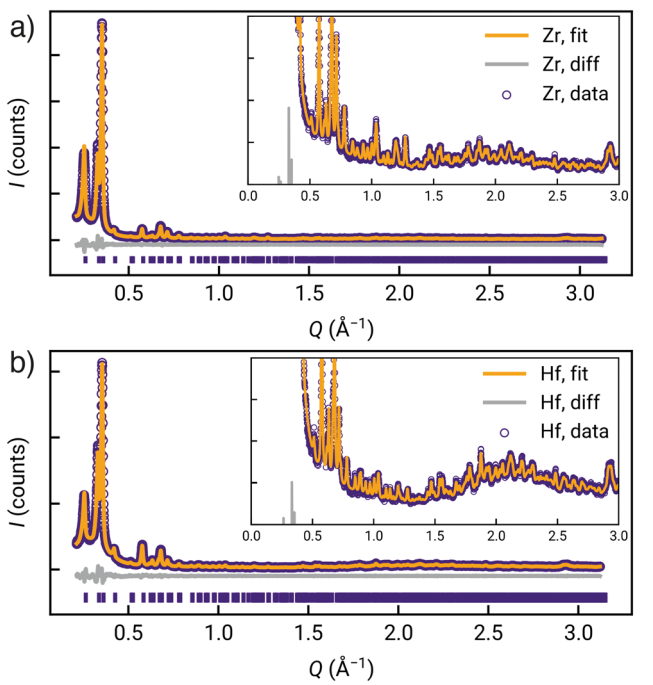

Fig. 3 Quantitative Pawley fitting (with insets to show low intensity reflections) of the powder X-ray diffractograms of a) GUF-12(Zr) and b) GUF-12(Hf).

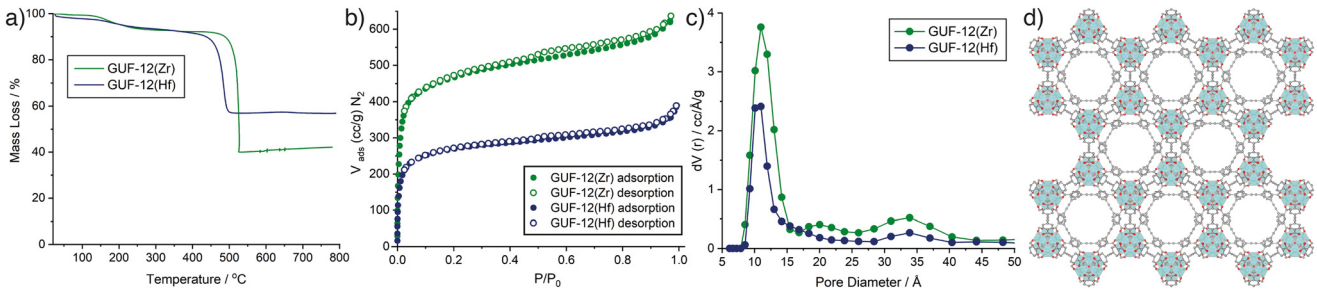

Fig. 4 a) Thermogravimetric analyses of GUF-12(Zr) and GUF-12(Hf) in air. b) N_2 adsorption desorption isotherms (77 K) of GUF-12(Zr) and GUF-12(Hf) with c) pore-size distributions (N_2 at 77 K on carbon, slit pore, QSDFT, equilibrium model) calculated from the isotherms. d) Portion of the DFT model structure of GUF-12(Zr) viewed down the crystallographic *c* axis to visualise the hexagonal channel 11 Å in diameter.

subsequent TGA residue).[41] This is commensurate with ^{1}H NMR spectra of acid-digested samples (see ESI,† Section S5), which show the presence of acetate even after activation, indicating that the acetate groups are present as charge compensating defects rather than pore-bound solvents. Resonances that could be assigned to formate, produced by decomposition of DMF, were not observed in the materials.

A pristine defect-free **hcp** structure would have formula $[M_{12}O_8(OH)_{14}(EDB)_9]$. ^{1}H NMR spectroscopic analysis of activated, then acid-digested GUF-12(Zr) gives a 1 : 3.3 ratio of acetate to linker; assuming that one EDB^{2-} is replaced by two acetates gives a formula of $[Zr_{12}O_8(OH)_{14}(EDB)_{7.8}(CH_3COO)_{2.4}]$, which would leave a theoretical 42.5% wt ZrO_2 residue after thermogravimetric analysis, matching well with the observed 42.1% wt. For GUF-12(Hf), the acetate content measured by ^{1}H NMR spectroscopy is higher, at an approximate 1 : 2.5 acetate to EDB^{2-} ratio. Similar levels of defectivity have been observed elsewhere for the **hcp** phase prepared from Zr(IV) and BDC^{2-} using acetic acid modulated syntheses; these defects enhance its catalytic activity.[33] Taking a similar approach, a formula of $[Hf_{12}O_8(OH)_{14}(EDB)_{7.5}(CH_3COO)_{3.0}]$ for GUF-12(Hf) would correlate with the NMR spectroscopic data and leave a theoretical HfO_2 residue of 56.3% wt, close to the experimental value of 56.8% wt. This greater acetate incorporation of the Hf(IV) congener may be reflected in its lower overall thermal decomposition temperature compared to the Zr(IV) analogue, as observed by TGA (Fig. 4a). The decomposition temperatures are broadly similar to the **fcu** analogues.[13]

The reliability of the synthetic method allowed us to upscale the synthesis of the **hcp** phases to quantities suitable for porosity analysis. N_2 adsorption/desorption isotherms of GUF-12(Zr) and GUF-12(Hf) were collected at 77 K after activation of the samples at 120 °C for 20 h under vacuum (Fig. 4b). Both MOFs exhibit typical type I isotherms, associated with microporous materials, with small increases in uptake between 0.9 and 1.0 P/P_0, indicating adsorption occurring in interparticle spacing or surface roughness. This can be explained by the aggregated "desert rose" morphology of the ~100 nm thick hexagonal particles, which feature multiple surfaces and crevices where nitrogen can be adsorbed. Brunauer–Emmett–Teller (BET) areas were calculated from the experimental adsorption isotherms using BETSI, a publicly available software package that fully implements the extended Rouquerol criteria for an unambiguous BET area assignment (see ESI,† Section S6).[44] The BET areas were found to be 1798 $m^2\ g^{-1}$ and 1005 $m^2\ g^{-1}$ for GUF-12(Zr) and GUF-12(Hf), respectively, with pore volumes of 1.03 $cm^3\ g^{-1}$ and 0.59 $cm^3\ g^{-1}$. As expected,[30,35] these are lower than those reported for the **fcu** analogues (3280 $m^2\ g^{-1}$ and 2000 $m^2\ g^{-1}$, for the Zr and Hf congeners, respectively).[13] Grand Canonical Monte Carlo (GCMC) simulations were performed to assess the potential total porosity of the two MOFs (see ESI,† Section S7). Simulated N_2 adsorption isotherms for both GUF-12(Zr) and GUF-12(Hf) showed higher N_2 uptakes and larger predicted BET areas (2765 $m^2\ g^{-1}$ and 2127 $m^2\ g^{-1}$, for the Zr and Hf congeners, respectively). GCMC simulations often overpredict porosity compared to experiment, but the magnitude of the difference between the experimental and simulated N_2 uptakes suggest that the isolated MOFs may be partially amorphized or not fully activated.

In each isotherm, small type H4 hysteresis loops are discernible, which are indicative of minor levels of mesoporosity that could be a consequence of defectivity in the samples. Pore-size distributions (Fig. 4c), calculated from the experimental isotherms (N_2 on carbon at 77 K, slit pore/QSDFD equilibrium) show a significant pore around 11 Å in diameter for each MOF, which correlates closely to the hexagonal pore evident along the crystallographic *c* axis (Fig. 4d), and is smaller than the major pore observed in the **fcu** analogues (~12.5 Å).[13] A broad feature is observed around 34 Å for each **hcp** MOF, which may be indicative of the defectivity implied by ^{1}H NMR spectroscopy and TGA. This combination of high porosity and significant defectivity indicates the potential for application of the GUF-12 congeners in catalysis.[33]

We and others have previously shown that MOFs linked by ligands with internal alkene[12,45–48] and alkyne[12,13,49,50] subunits can be postsynthetically modified by halogenation. Specifically, we have demonstrated that the Zr(IV) and Hf(IV) **fcu** phases linked by EDB^{2-} can be quantitatively brominated in a single-crystal to single-crystal manner.[13] With two different linker environments in the **hcp** phases in this work,

we wished to determine if (i) the linkers were accessible to bromination, and (ii) if this would result in a reactive delamination to form a nanosheet phase. Under conditions identical to those we have previously utilised for the **fcu** analogue,[13] it was possible to quantitatively brominate the EDB^{2-} ligands of the **hcp** materials, as assessed by ^{1}H and ^{13}C NMR spectroscopy of acid-digested samples. However, PXRD analysis of the brominated materials showed that stability was an issue when samples were scaled up, with inconsistent results. In the case of GUF-12(Hf), additional Bragg reflections were present that may represent degradation of the MOF or delamination, underlining the metastability of the **hcp** MOFs (see ESI,† Section S8).

Conclusions

We have shown that, by careful consideration of synthetic conditions, it is possible to synthesise Zr(IV) and Hf(IV) MOFs of EDB^{2-} with the **hcp** topology to complement their established **fcu** analogues. The role of both water and acetic acid has been explored to optimise syntheses and reliably reproduce the materials on an increased scale, allowing characterisation of their porosity and possible defectivity, suggesting potential applications in heterogeneous catalysis. The **hcp** phases are likely kinetic products relative to the analogous **fcu** topology MOFs; moreover, the **hcp** materials are metastable, as demonstrated by partial degradation of GUF-12(Hf) during attempts to postsynthetically brominate the EDB^{2-} linkers, in contrast to the stability of the **fcu** phase under identical conditions.[13] Nevertheless, this work shows that careful control of modulated self-assembly allows access to new MOF materials exhibiting desirable physical properties within well-established phase spaces.

Conflicts of interest

There are no conflicts to declare.

Acknowledgements

R. S. F. thanks the Royal Society for receipt of a URF and the University of Glasgow for funding. The work has been supported by the European Research Council (ERC) under the European Union's Horizon 2020 Programme for Research and Innovation (R. S. F.: grant agreement no. 677289, SCoTMOF, ERC-2015-STG; D. F. J.: grant agreement no. 726380, NanoMOFdeli, ERC-2016-COG). M. J. C. thanks the School of Chemistry at the University of Nottingham for receipt of a Hobday Fellowship. M. R. A. K. acknowledges support from the Cambridge Trust Scholarship and the Trinity-Henry Barlow Scholarship. We acknowledge the use of the ARCHER2 supercomputer through membership of the UK's HPC Materials Chemistry Consortium, which is funded by EPSRC grant no. EP/R029431. The data which underpin this submission are free to dowload at **https://dx.doi.org/10.5525/gla.researchdata.1406**.

References

1 H. Furukawa, K. E. Cordova, M. O'Keeffe and O. M. Yaghi, *Science*, 2013, **341**, 1230444.
2 P. Z. Moghadam, A. Li, X.-W. Liu, R. Bueno-Perez, S.-D. Wang, S. B. Wiggin, P. A. Wood and D. Fairen-Jimenez, *Chem. Sci.*, 2020, **11**, 8373–8387.
3 R. Freund, S. Canossa, S. M. Cohen, W. Yan, H. Deng, V. Guillerm, M. Eddaoudi, D. G. Madden, D. Fairen-Jimenez, H. Lyu, L. K. Macreadie, Z. Ji, Y. Zhang, B. Wang, F. Haase, C. Wöll, O. Zaremba, J. Andreo, S. Wuttke and C. S. Diercks, *Angew. Chem., Int. Ed.*, 2021, **60**, 23946–23974.
4 C. Ma, L. Zheng, G. Wang, J. Guo, L. Li, Q. He, Y. Chen and H. Zhang, *Aggregate*, 2022, **3**, e145.
5 T. Devic and C. Serre, *Chem. Soc. Rev.*, 2014, **43**, 6097–6115.
6 R. S. Forgan, *Chem. Sci.*, 2020, **11**, 4546–4562.
7 D. Bara, E. Meekel, I. Pakamore, C. Wilson, S. Ling and R. S. Forgan, *Mater. Horiz.*, 2021, **8**, 3377–3386.
8 Y. Bai, Y. Dou, L.-H. Xie, W. Rutledge, J.-R. Li and H.-C. Zhou, *Chem. Soc. Rev.*, 2016, **45**, 2327–2367.
9 J. H. Cavka, S. Jakobsen, U. Olsbye, N. Guillou, C. Lamberti, S. Bordiga and K. P. Lillerud, *J. Am. Chem. Soc.*, 2008, **130**, 13850–13851.
10 A. Schaate, P. Roy, T. Preuße, S. J. Lohmeier, A. Godt and P. Behrens, *Chem. – Eur. J.*, 2011, **17**, 9320–9325.
11 J. Lippke, B. Brosent, T. von Zons, E. Virmani, S. Lilienthal, T. Preuße, M. Hülsmann, A. M. Schneider, S. Wuttke, P. Behrens and A. Godt, *Inorg. Chem.*, 2017, **56**, 748–761.
12 R. J. Marshall, S. L. Griffin, C. Wilson and R. S. Forgan, *Chem. – Eur. J.*, 2016, **22**, 4870–4877.
13 R. J. Marshall, S. L. Griffin, C. Wilson and R. S. Forgan, *J. Am. Chem. Soc.*, 2015, **137**, 9527–9530.
14 M. Schulz, N. Marquardt, M. Schäfer, D. P. Warwas, S. Zailskas and A. Schaate, *Chem. – Eur. J.*, 2019, **25**, 13598–13608.
15 X. Li, J. Xie, Z. Du, L. Jiang, G. Li, S. Ling and K. Zhu, *Chem. Sci.*, 2022, **13**, 6291–6296.
16 M. Perfecto-Irigaray, G. Beobide, O. Castillo, I. da Silva, D. García-Lojo, A. Luque, A. Mendia and S. Pérez-Yáñez, *Chem. Commun.*, 2019, **55**, 5954–5957.
17 V. Bon, I. Senkovska, M. S. Weiss and S. Kaskel, *CrystEngComm*, 2013, **15**, 9572–9577.
18 M. J. Cliffe, W. Wan, X. Zou, P. A. Chater, A. K. Kleppe, M. G. Tucker, H. Wilhelm, N. P. Funnell, F.-X. Coudert and A. L. Goodwin, *Nat. Commun.*, 2014, **5**, 4176.
19 D. N. Johnstone, F. C. N. Firth, C. P. Grey, P. A. Midgley, M. J. Cliffe and S. M. Collins, *J. Am. Chem. Soc.*, 2020, **142**, 13081–13089.
20 V. Guillerm, F. Ragon, M. Dan-Hardi, T. Devic, M. Vishnuvarthan, B. Campo, A. Vimont, G. Clet, Q. Yang, G. Maurin, G. Férey, A. Vittadini, S. Gross and C. Serre, *Angew. Chem., Int. Ed.*, 2012, **51**, 9267–9271.
21 V. V. Butova, A. P. Budnyk, K. M. Charykov, K. S. Vetlitsyna-Novikova, C. Lamberti and A. V. Soldatov, *Chem. Commun.*, 2019, **55**, 901–904.

22 F. C. N. Firth, M. W. Gaultois, Y. Wu, J. M. Stratford, D. S. Keeble, C. P. Grey and M. J. Cliffe, *J. Am. Chem. Soc.*, 2021, **143**, 19668–19683.
23 M. J. Cliffe, E. Castillo-Martínez, Y. Wu, J. Lee, A. C. Forse, F. C. N. Firth, P. Z. Moghadam, D. Fairen-Jimenez, M. W. Gaultois, J. A. Hill, O. V. Magdysyuk, B. Slater, A. L. Goodwin and C. P. Grey, *J. Am. Chem. Soc.*, 2017, **139**, 5397–5404.
24 A. A. Bezrukov, K. W. Törnroos, E. Le Roux and P. D. C. Dietzel, *Chem. Commun.*, 2018, **54**, 2735–2738.
25 S. Waitschat, H. Reinsch and N. Stock, *Chem. Commun.*, 2016, **52**, 12698–12701.
26 S. Waitschat, H. Reinsch, M. Arpacioglu and N. Stock, *CrystEngComm*, 2018, **20**, 5108–5111.
27 S. Leubner, V. E. G. Bengtsson, K. Synnatschke, J. Gosch, A. Koch, H. Reinsch, H. Xu, C. Backes, X. Zou and N. Stock, *J. Am. Chem. Soc.*, 2020, **142**, 15995–16000.
28 M. Ermer, J. Mehler, M. Kriesten, Y. S. Avadhut, P. S. Schulz and M. Hartmann, *Dalton Trans.*, 2018, **47**, 14426–14430.
29 L. Zhou, F. Liu, J. Wang, R. Chen and Y. Chen, *CrystEngComm*, 2021, **23**, 2961–2967.
30 F. C. N. Firth, M. J. Cliffe, D. Vulpe, M. Aragones-Anglada, P. Z. Moghadam, D. Fairen-Jimenez, B. Slater and C. P. Grey, *J. Mater. Chem. A*, 2019, **7**, 7459–7469.
31 B. Moll, T. Müller, C. Schlüsener, A. Schmitz, P. Brandt, S. Öztürk and C. Janiak, *Mater. Adv.*, 2021, **2**, 804–812.
32 S. B. Peh, Y. Cheng, J. Zhang, Y. Wang, G. H. Chan, J. Wang and D. Zhao, *Dalton Trans.*, 2019, **48**, 7069–7073.
33 X. Chen, Y. Lyu, Z. Wang, X. Qiao, B. C. Gates and D. Yang, *ACS Catal.*, 2020, **10**, 2906–2914.
34 R. Dai, F. Peng, P. Ji, K. Lu, C. Wang, J. Sun and W. Lin, *Inorg. Chem.*, 2017, **56**, 8128–8134.
35 P. Ji, K. Manna, Z. Lin, X. Feng, A. Urban, Y. Song and W. Lin, *J. Am. Chem. Soc.*, 2017, **139**, 7004–7011.
36 M. R. Momeni and C. J. Cramer, *Chem. Mater.*, 2018, **30**, 4432–4439.
37 Y.-Y. Zhu, G. Lan, Y. Fan, S. S. Veroneau, Y. Song, D. Micheroni and W. Lin, *Angew. Chem., Int. Ed.*, 2018, **57**, 14090–14094.
38 K. Lu, C. He, N. Guo, C. Chan, K. Ni, G. Lan, H. Tang, C. Pelizzari, Y. X. Fu, M. T. Spiotto, R. R. Weichselbaum and W. Lin, *Nat. Biomed. Eng.*, 2018, **2**, 600–610.
39 L. Zhou, S. Wang, Y. Chen and C. Serre, *Microporous Mesoporous Mater.*, 2019, **290**, 109674.
40 X.-L. Lv, M. Tong, H. Huang, B. Wang, L. Gan, Q. Yang, C. Zhong and J.-R. Li, *J. Solid State Chem.*, 2015, **223**, 104–108.
41 I. Abánades Lázaro and R. S. Forgan, *Coord. Chem. Rev.*, 2019, **380**, 230–259.
42 T. Gadzikwa, B.-S. Zeng, J. T. Hupp and S. T. Nguyen, *Chem. Commun.*, 2008, 3672–3674.
43 A. A. Coelho, J. Evans, I. Evans, A. Kern and S. Parsons, *Powder Diffr.*, 2011, **26**, S22–S25.
44 J. W. M. Osterrieth, J. Rampersad, D. Madden, N. Rampal, L. Skoric, B. Connolly, M. D. Allendorf, V. Stavila, J. L. Snider, R. Ameloot, J. Marreiros, C. Ania, D. Azevedo, E. Vilarrasa-Garcia, B. F. Santos, X.-H. Bu, Z. Chang, H. Bunzen, N. R. Champness, S. L. Griffin, B. Chen, R.-B. Lin, B. Coasne, S. Cohen, J. C. Moreton, Y. J. Colón, L. Chen, R. Clowes, F.-X. Coudert, Y. Cui, B. Hou, D. M. D'Alessandro, P. W. Doheny, M. Dincă, C. Sun, C. Doonan, M. T. Huxley, J. D. Evans, P. Falcaro, R. Ricco, O. Farha, K. B. Idrees, T. Islamoglu, P. Feng, H. Yang, R. S. Forgan, D. Bara, S. Furukawa, E. Sanchez, J. Gascon, S. Telalović, S. K. Ghosh, S. Mukherjee, M. R. Hill, M. M. Sadiq, P. Horcajada, P. Salcedo-Abraira, K. Kaneko, R. Kukobat, J. Kenvin, S. Keskin, S. Kitagawa, K.-I. Otake, R. P. Lively, S. J. A. DeWitt, P. Llewellyn, B. V. Lotsch, S. T. Emmerling, A. M. Pütz, C. Martí-Gastaldo, N. M. Padial, J. García-Martínez, N. Linares, D. Maspoch, J. A. Suárez del Pino, P. Moghadam, R. Oktavian, R. E. Morris, P. S. Wheatley, J. Navarro, C. Petit, D. Danaci, M. J. Rosseinsky, A. P. Katsoulidis, M. Schröder, X. Han, S. Yang, C. Serre, G. Mouchaham, D. S. Sholl, R. Thyagarajan, D. Siderius, R. Q. Snurr, R. B. Goncalves, S. Telfer, S. J. Lee, V. P. Ting, J. L. Rowlandson, T. Uemura, T. Iiyuka, M. A. van der Veen, D. Rega, V. Van Speybroeck, S. M. J. Rogge, A. Lamaire, K. S. Walton, L. W. Bingel, S. Wuttke, J. Andreo, O. Yaghi, B. Zhang, C. T. Yavuz, T. S. Nguyen, F. Zamora, C. Montoro, H. Zhou, A. Kirchon and D. Fairen-Jimenez, *Adv. Mater.*, 2022, **34**, 2201502.
45 C. A. Walshe, A. J. R. Thom, C. Wilson, S. Ling and R. S. Forgan, *Chem. – Eur. J.*, 2022, **28**, e202201364.
46 R. J. Marshall, T. Richards, C. L. Hobday, C. F. Murphie, C. Wilson, S. A. Moggach, T. D. Bennett and R. S. Forgan, *Dalton Trans.*, 2016, **45**, 4132–4135.
47 S. C. Jones and C. A. Bauer, *J. Am. Chem. Soc.*, 2009, **131**, 12516–12517.
48 T. J. Azbell, R. M. Mandel, J.-H. Lee and P. J. Milner, *ACS Appl. Mater. Interfaces*, 2022, **14**, 53928–53935.
49 D. Frahm, F. Hoffmann and M. Fröba, *Cryst. Growth Des.*, 2014, **14**, 1719–1725.
50 T. J. Matemb Ma Ntep, H. Reinsch, J. Liang and C. Janiak, *Dalton Trans.*, 2019, **48**, 15849–15855.